Computer simulation of liquid Al_2O_3

2006 J. Phys.: Condens. Matter 18 9309

(http://iopscience.iop.org/0953-8984/18/41/001)

INSTITUTE OF PHYSICS PUBLISHING JOURNAL OF PHYSICS: CONDENSED MATTER

J. Phys.: Condens. Matter **18** (2006) 9309–9322 doi:10.1088/0953-8984/18/41/001

Computer simulation of liquid Al_2O_3

P K Hung[1], L T Vinh[1], D M Nghiep[2] and P N Nguyen[1]

[1] Department of Computational Physics, Hanoi University of Technology, Vietnam
[2] Materials Science Center, Hanoi University of Technology, Vietnam

Received 19 July 2006, in final form 23 August 2006
Published 29 September 2006
Online at stacks.iop.org/JPhysCM/18/9309

Abstract

Molecular dynamic simulation has been done to determine the dynamic and local structure of liquid alumina at 3000 K. Fourteen different systems at densities ranging from 2.5 to 4.5 g cm^{-3} was prepared by compressing the low-density melt. Two kinds of pore aggregation, pore cluster and pore tube, were examined. Clear evidence was found of structural transformation from a tetrahedral to an octahedral network. For a low-density system there was a large pore tube, which involved 93% of oxygen-vacancy-like pores and spread over the whole simulation cell. Conversely, in a high-density system the largest pore tube contained less than 1% of all oxygen-vacancy-like pores. A similar trend also was observed for other pore kinds such as aluminium-vacancy-like pores and large pore clusters. The diffusion constants significantly decreased in the region of the structural transformation. The diffusion mechanism in low- and high-density systems was examined and is discussed here.

1. Introduction

In recent years, network-forming fluids such as SiO_2, GeO_2 and Al_2O_3 have been the objects of renewed interest because of a number of peculiar properties [1–16]. Experiments have shown that for silica liquid a range of pressure exists for which diffusivity increases and viscosity decreases upon compression [12]. Associated anomalies are also isobaric heat capacity minima and isothermal compressibility minima. According to data from *in situ* experiment [17], liquid GeO_2 consisting of four-coordinated germanium contrasted with increasing pressure without significant change in local structure up to 2.5 GPa, and then it showed an abrupt fourfold- to sixfold-coordination change around 3 GPa. These results indicated the existence of two distinct liquid states and the possibility of liquid–liquid phase transition.

Recently, considerable effort has been made to study the phase transition for liquid and glass under various mechanical and thermal conditions. Computer simulations are often employed to interpret experimental data and to understand the transition between low- and high-density phase and their structure. Gonzalo *et al* have done molecular dynamic (MD) simulation of liquid GeO_2 and found a volume collapse in the pressure–volume curve in the range of 4–8 GPa [2]. This result indicated the possibility of liquid–liquid transition. Other

MD simulations demonstrated that the densification is accompanied by a reduction in the ring size and a collapse of void space [5, 6].

For liquid Al_2O_3, only a few simulations have been done [6, 18–20, 23–26]. Sanmiguel *et al* [21] have performed a MD simulation for the Al_2O_3 system at temperatures from 2200 to 3000 K. They found that liquid structure is invariant as a function of temperature at constant volume and concluded that more than 50% of Al atoms are four coordinated. The structural transformation from a tetrahedral to an octahedral network in liquid alumina was found to occur at a density range of 3.6–4.5 g cm^{-3} [23, 24]. However, this structural transformation so far is not understood; in particular, the structural descriptions of the different liquid states are still very limited. In this context, the systematic study based on MD simulation in both dynamic and structural aspects can be useful in dealing with this matter. On the other hand, liquid alumina has many pores in which no atom exists, and the knowledge of the pore and its aggregation can be used to identify the topological changes that occur under structural transformation. Nevertheless, up to now there is no study about the pore and its aggregation in liquid Al_2O_3. Therefore, in the present work, 14 liquid Al_2O_3 models with different densities ranging from 2.5 to 4.5 g cm^{-3} and at 3000 K have been constructed and examined in order to give more detailed information about both the local structure and dynamic of liquid Al_2O_3 under compression. Special analysis is given to the pore and its aggregation.

2. Details of simulations

MD simulation of the Al_2O_3 system containing 2000 atoms in the basic cube with periodic boundary conditions is carried out. A major issue in MD simulation is the choice of the interaction potential. A number of potentials have been developed to study the Al_2O_3 system [5, 6, 23, 24]. In the current work we used the Born–Mayer type pair potential, which is still simple and reproduces a number of experimental properties such as structure, density and thermal expansivity in amorphous and liquid states [5]. The potential is given as

$$u_{ij}(r) = z_i z_j \frac{e^2}{r} + B_{ij} \exp\left(-\frac{r}{R_{ij}}\right). \tag{1}$$

Here r is the distance between centres of the ith and jth ions; z_i and z_j are the charges of the ith and jth ions; B_{ij} and R_{ij} are the parameters accounting for the repulsion of the ionic cells. The values $z_1 = +3$ and $z_2 = -2$ are the charges of Al^{3+} and O^{2-}. The values $B_{11} = 0$, $B_{12} = 1479.86$, $B_{22} = 1500$ eV and $R_{ij} = 3.4483$ Å were close to ones in [5]. The long-range Coulomb interactions are calculated with the standard Ewald technique. We used the Verlet algorithm to integrate the motion equation. The MD time step is equal to 0.4 fs. The initial configuration of the system was obtained by randomly placing all atoms in the simulation box. This configuration is heated to 5000 K and treated over 50 000 steps. After this, the sample is cooled down to 3000 K and then held at fixed temperature within 200 000 MD steps. Next, with this low-density melt, we have prepared 14 systems with different density (different pressure) ranging from 2.5 to 4.25 g cm^{-3}. After each volume change, the system was relaxed over 100 000 MD steps at constant temperature and pressure (i.e. NPT simulation), then we relaxed the obtained model by 100 000 further steps at constant volume ensemble (i.e. NVE simulation). After this the dynamic and structural characteristics were determined. In order to improve statistics, all positional and angular characteristics were calculated by performing the average over the last 1000 configurations separated by ten steps.

If every atom is considered as a sphere, then there is a part of the system in which no atomic sphere exists. The radii of Al and O atoms are 1.23 and 0.73 Å respectively. The pore is defined as a sphere that can be inserted in contact with four atoms and does not intersect

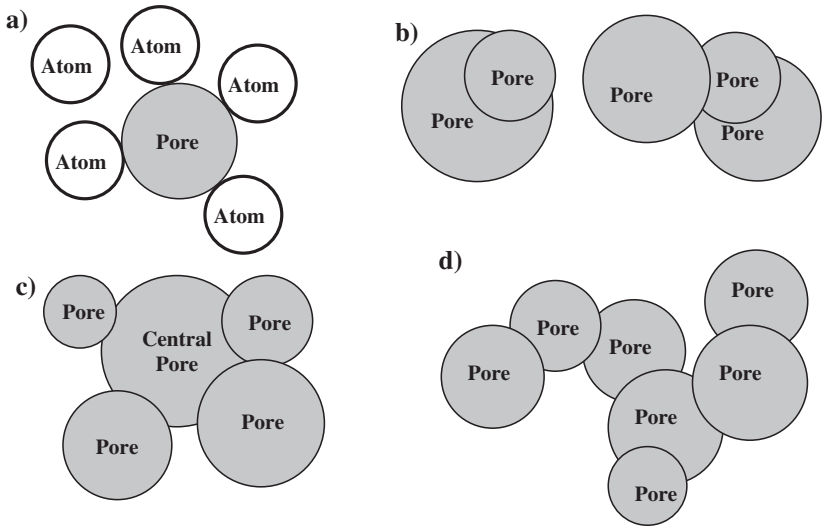

Figure 1. Pore and pore aggregation: (a) pore and neighbour atoms; (b) small pore located almost in large pore (left) and in two nearest pores (right)—these pores will be removed from the system; (c) pore cluster; (d) pore tube.

with any atom (see figure 1(a)). In previous work [22], an additional lattice was embedded in the system to calculate the pore set. This method is poorly accurate and less efficient. In the present work, we used the following algorithm: firstly, we took all sets of four atoms in the system with the condition that the distance between any two of them was less than 9.5 Å. Then a pore sphere was inserted in contact with these four atomic spheres. If the inserted pore is overlapped with any atom, it will be removed from the system. Thereby, we obtained a set of pores, which are not intersected with any atom. Among the obtained pores, some may be located almost inside other pores or several nearest pores (see figure 1(b)). The next step is to remove these pores from the system. To remove them, two million points were randomly generated in the simulation cell. For every ith pore, we determined the number of points n_i located inside the ith pore. Then the number of points n_{2i} in both the ith pore and another bigger pore was calculated. The ith pore is removed if the relation n_{2i}/n_i is bigger than 0.95.

3. Results and discussion

3.1. Atomic correlation

Figure 2 showed the calculated total radial distribution function (RDF) for the liquid model and experimental data from [3]. Although there was a small discrepancy around the first peak in the RDF (see figure 2), it agreed well with experiment. An overview of the performed simulation is given in figure 3, displaying the pressure–density relation. The structural characteristics of obtained models are summarized in table 1. The major change we can notice here is a decrease in the height of the first peak of the RDF, g_{ij}, for the Al–O pair as pressure increases. For other pairs the opposite tendency of g_{ij} was obtained. From the positions of the first peak of the RDF, r_{ij}, we found that the Al–O bond length slightly rose with pressure, whereas the nearest neighbour distance for O–O and Al–Al pairs reduced (see table 1).

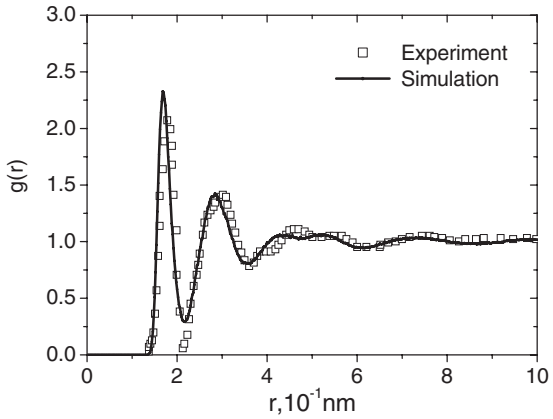

Figure 2. The total radial distribution function of liquid Al_2O_3.

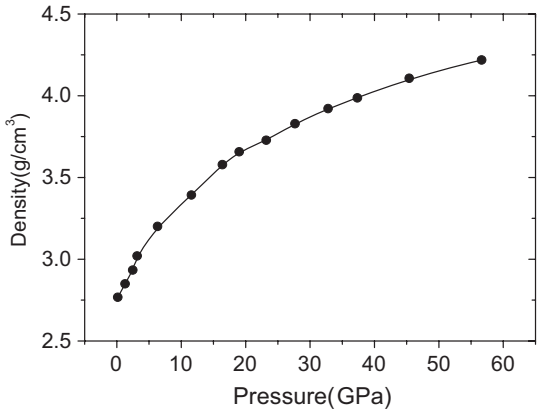

Figure 3. Density versus pressure for alumina liquid.

The tetrahedral network structure of the system can be seen through the mean coordination number and the proportion of basic units AlO_x ($x = 2, 3, \ldots, 7$). To calculate the coordination number we used the cut-off distances, chosen as the positions of the minimum after the first peak in the RDFs. According to [8, 24] the liquid Al_2O_3 has the structure of a tetrahedral network with averaged coordination number ∼4. The basic unit of this network is a slightly distorted tetrahedron AlO_4. The same structure also exists in our model at 0.14 GPa. In this model the Al atoms are mainly surrounded by four oxygen atoms.

As shown from table 1 the mean coordination number for the Al–O pair changed from 4.31 in the low-density (LD) to 5.92 in the high-density (HD) system, clearly indicating the structural transition from tetrahedral to octahedral network. This is slightly different from results in [24], where a mean coordination number of 5.7 was found for the HD model. The discrepancy is probably caused by different cut-off distances and potentials.

The dependence of proportion of basic units on pressure is displayed in figure 4. As mentioned in [8, 24], besides AlO_4, the liquid Al_2O_3 has a considerable amount of AlO_5. We also found a large amount of AlO_5. Its fraction was 0.28 at 0.14 GPa and increased to 0.53 at 11.58 GPa and then decreased with pressure (see figure 4). From figure 4 one can notice

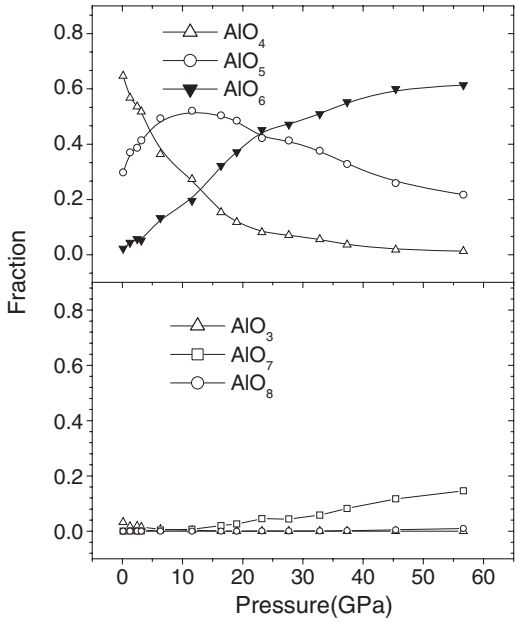

Figure 4. The dependence of AlO_x proportion on pressure for liquid alumina.

Table 1. Structural characteristics of liquid alumina. r_{ij}, g_{ij}—the position and height of the first peak in the partial RDFs; Z_{ij}—the averaged coordination number. Here 1–1 is for the Al–Al pair; 1–2 for the Al–O pair; 2–1 for the O–Al pair; 2–2 for the O–O pair.

Pressure	r_{ij} (Å)			g_{ij}			Z_{ij}			
(GPa)	1–1	1–2	2–2	1–1	1–2	2–2	1–1	1–2	2–1	2–2
0.14	3.14	1.70	2.78	2.87	5.73	2.36	7.93	4.31	2.87	10.54
1.28	3.14	1.70	2.76	2.82	5.61	2.34	8.16	4.44	2.96	11.08
2.47	3.10	1.70	2.74	2.84	5.42	2.36	8.67	4.48	2.99	11.64
3.16	3.14	1.70	2.76	2.77	5.30	2.32	9.05	4.51	3.00	12.00
6.32	3.10	1.70	2.72	2.78	5.05	2.31	9.99	4.76	3.17	12.34
11.58	3.06	1.72	2.68	2.83	4.85	2.33	10.92	4.93	3.29	13.43
16.38	3.06	1.72	2.62	2.85	4.58	2.40	12.08	5.21	3.47	13.65
19.01	3.04	1.74	2.60	2.89	4.51	2.43	12.16	5.31	3.54	14.46
23.20	3.04	1.74	2.56	2.87	4.49	2.42	12.45	5.46	3.64	14.73
27.66	3.02	1.74	2.54	2.92	4.46	2.49	12.69	5.49	3.66	15.01
32.80	3.02	1.74	2.56	2.94	4.39	2.46	12.76	5.57	3.71	14.98
37.35	3.02	1.72	2.56	2.90	4.37	2.57	12.81	5.69	3.79	15.64
45.41	2.94	1.74	2.54	2.88	4.32	2.61	13.12	5.83	3.89	15.97
56.65	2.90	1.74	2.50	2.96	4.33	2.62	13.06	5.92	3.95	15.96

that a significant change in structure occurred at 5–12 GPa. In this region the structure of the tetrahedral network, in which the AlO_4 and AlO_5 are in the majority, was rearranged and transformed to an octahedral network consisting mainly of AlO_5 and AlO_6.

Useful information about the local structure in the liquid is provided by bond-angle distribution. Here we calculated only O–Al–O and Al–O–Al bond-angles. The first bond-

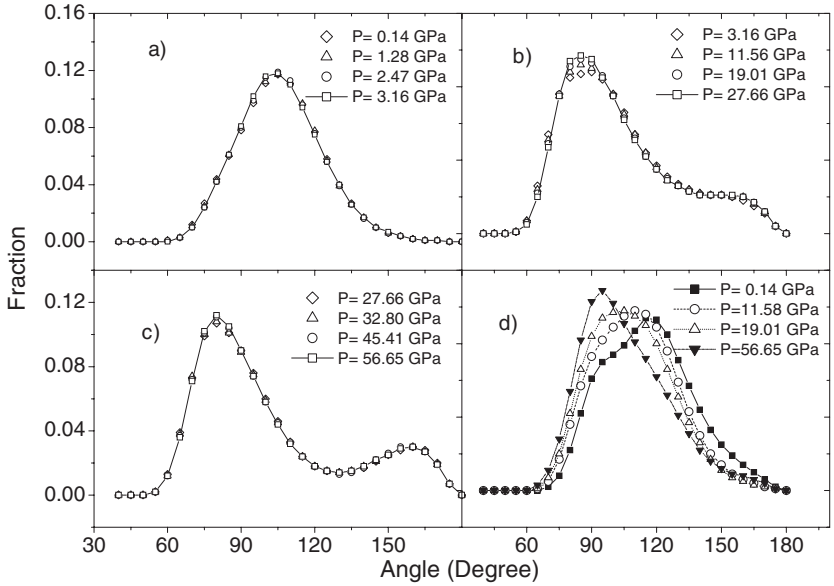

Figure 5. The bond-angle distribution for liquid alumina: (a) for O–Al–O in AlO_4; (b) for O–Al–O in AlO_5; (c) for O–Al–O in AlO_6 and (d) for Al–O–Al between two adjacent AlO_x.

angle described the short-range order (SRO) inside the basic units and the second one provided the connectivity between them. Obviously, we can identify the change of SRO in basic units from these bond-angle distributions. As shown in [8], the O–Al–O bond-angle distribution for Al_2O_3 liquid strongly changed with density. This result could not give detailed information about the SRO of basic units, because the O–Al–O bond-angle distribution in [8] was obtained by performing an average over all basic units in the system and the proportion of them also strongly changed with density. In the current work we separately calculated the bond-angle distribution for each kind among AlO_4, AlO_5 and AlO_6, and our calculation gives different results from those in [8, 24].

Figure 5 displays O–Al–O bond-angle distributions for liquid alumina. We can see a pronounced peak appeared at 108° for the O–Al–O bond-angle distribution of the AlO_4 polyhedron. These data indicated a slightly distorted tetrahedron with an aluminium atom at the centre and four oxygen atoms at the vertices. For AlO_5 and AlO_6 there are two peaks: the main peak is located at 88° and a small one at 164°. It can be seen that O–Al–O bond-angle distributions are unchanged with pressure. Therefore, the structural transformation was accompanied by a strong change with proportion of basic units and unchanged in SRO for AlO_4, AlO_5 and AlO_6 units.

For the Al–O–Al angle, we also observed a peak and its height gradually decreased with pressure (see figure 5). Furthermore, this peak shifted from 120° to 92° as pressure increased from 0.14 to 56.65 GPa. For the LD system, a small shoulder appeared, reflecting the strong change in the connectivity between two adjacent basic units.

Interesting information about the connectivity between two adjacent basic units also can be inferred from the distribution of 'bridge oxygen' presented in table 2. Two adjacent units AlO_x are linked to each other by a common oxygen atom, which is called 'bridge oxygen'. According to table 2, most of the connectivity consisted of one and two bridge-oxygen atoms. The fraction of different connectivities (one, two or three bridge-oxygen connectivities) also

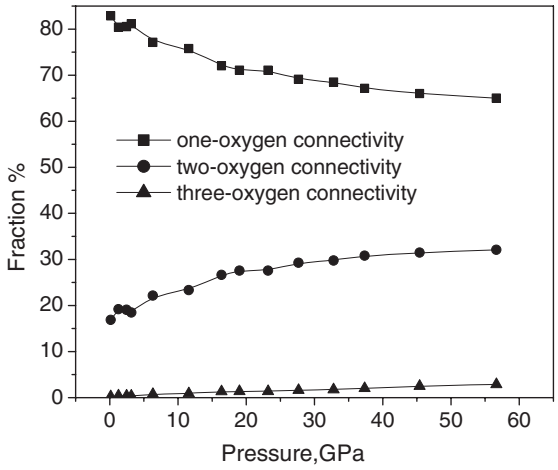

Figure 6. The dependence of proportion of different bridge-oxygen connectivities on pressure.

Table 2. The distribution of 'bridge oxygen' in liquid alumina. m is the number of bridge-oxygen atoms that two adjacent units AlO_x are bonded to. The next columns indicate the percentage of connectivities. For example, at 1.28 GPa 19.201% of connectivities have two bridge-oxygen atoms.

Pressure	m				
(GPa)	1	2	3	4	5
0.14	82.883	16.886	0.232	0.000	0.000
1.28	80.397	19.201	0.402	0.000	0.000
2.47	80.545	19.058	0.397	0.000	0.000
3.16	81.162	18.476	0.362	0.000	0.000
6.32	77.117	22.149	0.733	0.001	0.000
11.58	75.768	23.349	0.882	0.000	0.000
16.38	72.043	26.641	1.315	0.001	0.001
19.01	71.063	27.579	1.354	0.003	0.000
23.20	71.063	27.579	1.354	0.003	0.000
27.66	69.112	29.269	1.616	0.004	0.000
32.80	68.496	29.757	1.739	0.008	0.000
37.35	67.147	30.820	2.020	0.013	0.000
45.41	65.993	31.482	2.500	0.026	0.000
56.65	65.007	32.084	2.862	0.043	0.004

changed gradually with pressure and can be seen in figure 6. Because the proportion of basic units changed with pressure, the frequency of connectivity between different kinds of two adjacent basic units also varied with pressure; for example, the frequency of connectivity between two AlO_4 decreased as pressure increased, but in contrast the one between AlO_5 and AlO_6 increased with pressure (see figure 4). So, the gradual variation seen in figure 6 as well as in figure 5 is caused by the change in proportion of basic units. Combining these results with the above-mentioned data we come to the conclusion that the main structural change in liquid Al_2O_3 under pressure is the change in the proportion of basic units, which results in variation with Al–O–Al bond-angle distribution and fraction of different connectivities.

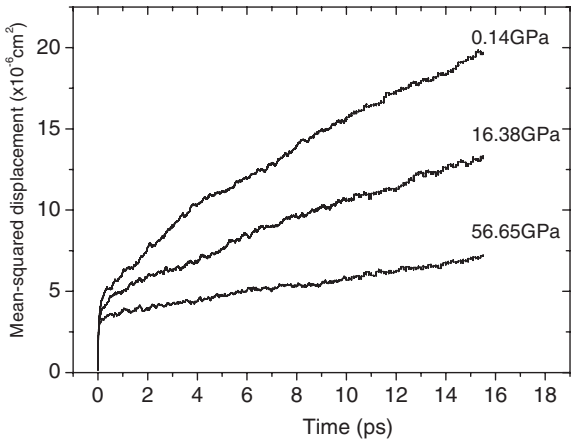

Figure 7. Mean-squared displacement versus time for liquid Al_2O_3.

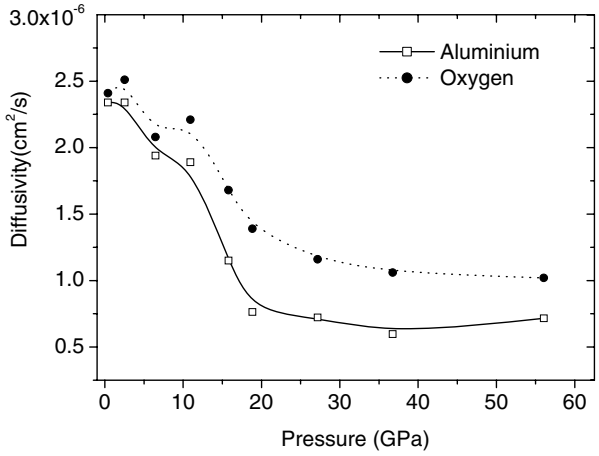

Figure 8. Self-diffusion coefficients versus pressure of aluminium and oxygen for Al_2O_3 liquid.

3.2. Dynamic property

The diffusion coefficient for components in the MD model can be calculated via the Einstein relation given below:

$$\lim_{t\to\infty} \frac{\langle r^2(t)\rangle}{6t} = D. \tag{2}$$

Graphs showing the mean-squared displacement $\langle r^2(t)\rangle$ with time are presented in figure 7. And the dependence of self-diffusion coefficients on pressure can be found in figure 8. It can be seen that the diffusion constants reduced significantly in the range of 5–15 GPa and then changed slightly with pressure. In this pressure range the structural transition from tetrahedral to octahedral network occurred.

In the pressure range of 15–56.65 GPa we observed a very small minimum in the aluminium diffusion constant–pressure curve. It is interesting to analyse the ratio between

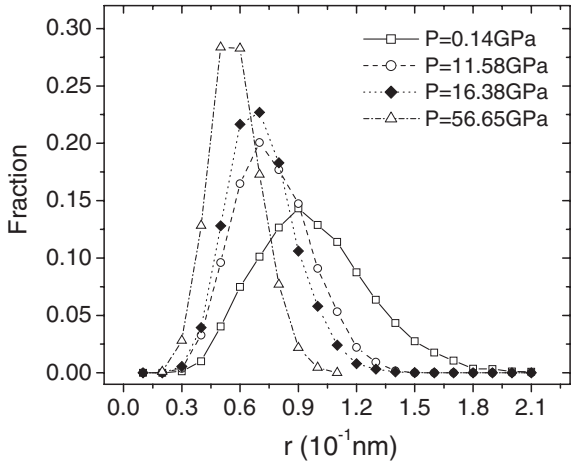

Figure 9. The radius distribution of pores.

the oxygen and aluminium diffusion constants. Figure 8 shows that the ratio D_{Al}/D_O changed from 1.0 at LD to 0.7 at HD. This data indicated the change in diffusion mechanism for LD and HD systems, which we will discuss in section 3.3.

3.3. Pores and pore clusters

The valuable information about the pore set in the system is the radius distribution of pores (RDP) shown in figure 9. We can see a pronounced peak and its position shifts to the left as the pressure increases. In particular, the position of the RDP peak changes from 0.9 for LD to 0.5 Å for HD. Generally, the shape of RDP strongly changes with pressure: the lower the pressure, the lower the height of the RDP peak and the wider the RDP. For the investigated pressure range, the height of the RDP reduced from 0.28 to 0.15.

The pores do not exist alone, but they can group into a cluster consisting of two or more pores. Two kinds of pore aggregation are examined: the pore cluster (PC) and pore tube (PT) (see figures 1(c) and (d)). The first one is a set of pores including a central pore and other smaller ones, which overlap with the central pore. The second one contains a number of pores with radius bigger than that of the oxygen atom, and every pore in the PT must overlap at least with one adjacent pore by a sharing circle. The radius of this circle is bigger than that of the oxygen atom. Obviously, from the viewpoint of the diffusion mechanism, the PT may serve as a diffusion path along which the oxygen can easy move. Some PCs and PTs detected in our models are presented in figure 10.

To give additional insight into pore aggregation, we have calculated the PC volume and the number of pores in one PC. The PC's volume is computed by generating 5000 points in a cube containing the PC inside. After this the total number of points n_{in} located in the PC is determined. The volume of the PC is calculated by $V_{PC} = V_{cube} \cdot n_{in}/5000$. Here V_{cube} is the volume of the cube, where 5000 points are randomly distributed. The PC volume distribution is listed in table 3. Here we found a number of very large PCs (the PC has large volume). For example, in the LD system (0.14 GPa) there are 41 PCs with volume five times bigger than V_{Al}, where $V_{Al} = 4\pi r_{Al}^3/3 = 8.18$ Å^3; r_{Al} is the aluminium radius. This means that the size of this PC is big enough that five aluminium atoms can be placed inside it. Obviously, this PC is very large and cannot be considered as a vacancy following the usual definition. More appropriately,

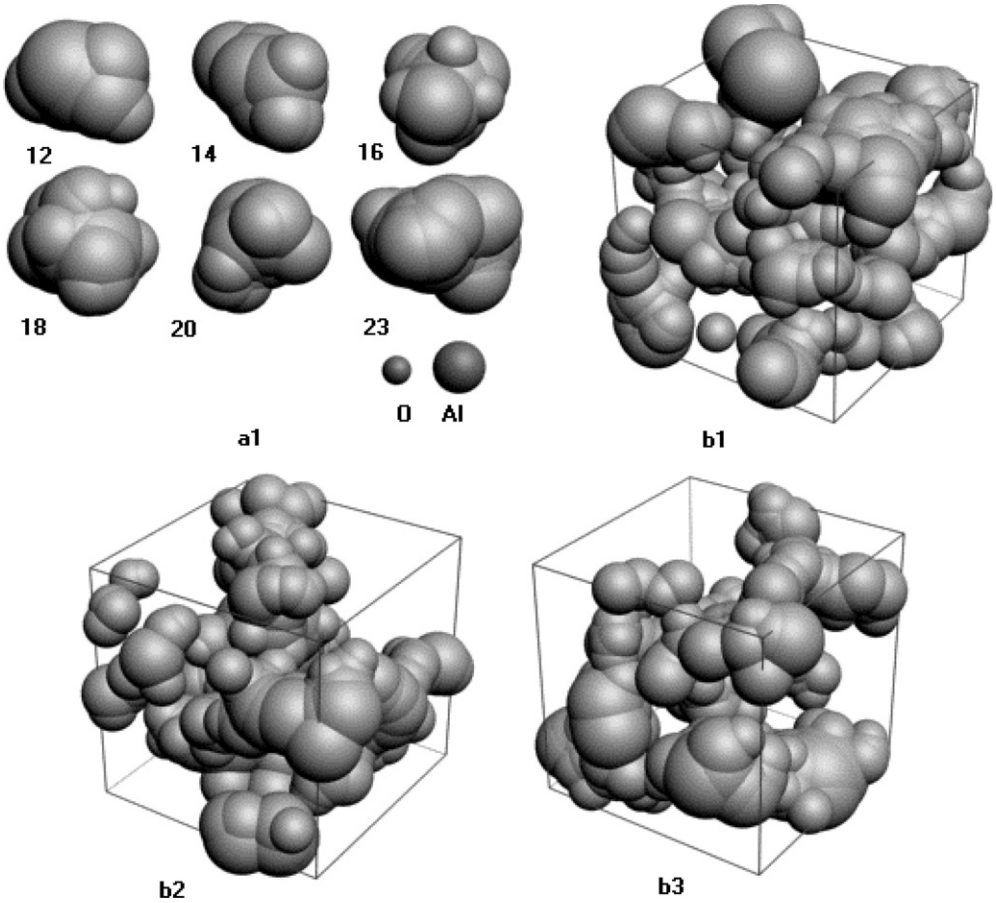

Figure 10. Some PCs (a1) and part of the largest PT in a cubic box with size of $10 \times 10 \times 10$ Å^3 in the simulation cell (b1, b2 and b3). Here b1, b2 and b3 correspond to the systems with densities of 2.767, 2.849 and 2.934 g cm^{-3} respectively. The numbers under the picture indicate the number of pores in PC.

it is a microscopic void. The number of these voids is significantly decreased with pressure (see table 3).

The distribution of PCs with different pore numbers is presented in table 4. The amount of pores in one PC characterizes the shape of the PC: the bigger the number of pores in the PC, the more complicated is its shape. Analogous to the case of PC volume, we also found a number of PCs having more than ten pores. In particular, at 16.38 GPa there are 122 PCs of this kind.

Figure 11 shows the dependence of volume fraction of different pore kinds on pressure. In addition to the above-considered pore kinds, we also calculated the number and volume fraction for oxygen-vacancy-like (OVPs) and aluminium-vacancy-like pores (AVPs). The OVPs and AVPs were considered as pores with radius bigger than those of oxygen and aluminium atoms respectively. From figure 11 we can make some remarks: firstly, the volume fraction of total pore number V_p and of OVPs V_{pO} gradually decreased as pressure increased from 0.14 to 56.65 GPa, whereas for AVPs and the largest PT the volume fraction significantly reduced in the range of 3–10 GPa. At 16.38 GPa, the volume fraction of AVPs and the largest PT was very small and could be neglected in comparison with others. Secondly, the ratio V_{pO}/V_p

Table 3. The volume distribution of PCs. The second row indicates the volume range from mV_{Al} to $(m+1)V_{Al}$. Here $m = 0, 1, 2, 10$, and V_{Al} is the volume of the Al atom. The following rows give the number of PCs. For example, at 1.28 GPa there are 235 PCs with the volume in the range of V_{Al}–$2V_{Al}$.

Pressure	Volume range ($*8.18$ Å^3)										
(GPa)	0–1	1–2	2–3	3–4	4–5	5–6	6–7	7–8	8–9	9–10	>10
0.14	1520	204	115	60	32	12	14	6	3	3	3
1.28	1657	235	99	59	33	14	9	4	0	2	1
2.47	1784	242	85	45	22	14	8	2	0	2	2
3.16	1871	275	90	48	20	6	2	2	1	0	0
6.32	2161	241	71	20	10	2	2	0	0	0	0
11.58	2383	239	53	5	2	0	0	0	0	0	0
16.38	2747	163	18	4	1	0	0	0	0	0	0
19.01	2904	157	10	1	0	0	0	0	0	0	0
23.20	3000	129	9	0	0	0	0	0	0	0	0
27.66	3099	92	1	0	0	0	0	0	0	0	0
32.80	3239	60	2	0	0	0	0	0	0	0	0
37.35	3348	54	1	0	0	0	0	0	0	0	0
45.41	3448	25	0	0	0	0	0	0	0	0	0
56.65	3586	14	0	0	0	0	0	0	0	0	0

Table 4. The distribution of PCs with different pore numbers. The second row indicates the range of pore numbers. The following rows show the number of PCs. For example, at 11.58 GPa there are 680 PCs containing from four to six pores.

Pressure	The range of pore number							
(GPa)	1–3	4–6	7–9	10–12	13–15	16–18	19–21	>21
0.14	1234	392	167	110	47	15	5	2
1.28	1314	436	194	94	57	14	4	0
2.47	1368	482	186	108	41	19	2	0
3.16	1409	497	242	115	43	8	1	0
6.32	1536	580	239	105	35	12	0	0
11.58	1606	680	262	111	19	4	0	0
16.38	1730	805	276	106	13	3	0	0
19.01	1854	836	287	82	12	1	0	0
23.20	1884	865	292	83	14	0	0	0
27.66	1937	854	318	76	6	1	0	0
32.80	1953	974	302	63	9	0	0	0
37.35	2051	1001	281	62	8	0	0	0
45.41	2058	1079	280	49	6	1	0	0
56.65	2205	1080	257	52	6	0	0	0

also decreased with pressure. In particular, its value is 0.95 for the LD system (0.14 GPa) and decreases to 0.40 for the HD system (56.65 GPa).

From table 5 one can see two opposite trends. First, the total number of all pores N_p and number of PCs N_{PC} increased with pressure. Second, the number of remaining pore kinds except number of PTs in contrast decreased as pressure increased from 0.14 to 56.65 GPa. Furthermore, we found one large PT in the LD system (0.14 GPa) contained 6368 OVPs, i.e. about 78% of all pores or 93% of all OVPs. Hence that PT was spread over whole system.

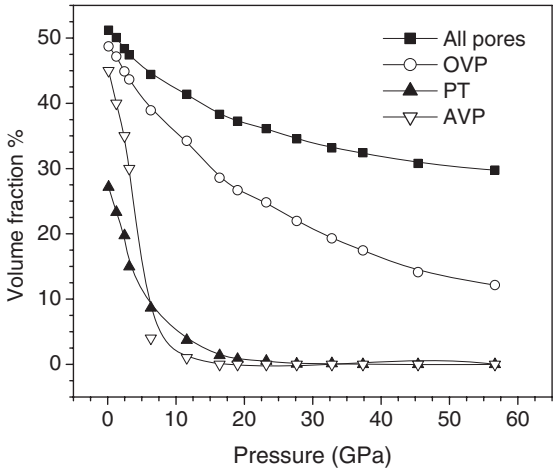

Figure 11. The dependence of volume fraction of different pore kinds on pressure.

Table 5. The characteristics of the pore and its aggregation. Here N_p, N_{pA}, N_{pO}, N_{PC}, N_{PT} and N_{pPT} are the numbers of all pores, AVPs, OVPs, PCs and PTs and the number of pores in the largest PT respectively.

Pressure (GPa)	N_p	N_{pO}	N_{pA}	N_{PC}	N_{PT}	N_{pPT}
0.14	8114	6866	1735	1972	250	6368
1.28	8419	6980	1497	2113	352	5937
2.47	8479	6746	1170	2206	383	5149
3.16	8729	6890	866	2315	462	4724
6.32	9306	6697	483	2507	653	606
11.58	9322	6004	188	2682	809	135
16.38	9696	5246	71	2933	933	65
19.01	9689	4860	42	3072	974	61
23.20	9630	4531	18	3138	983	38
27.66	9768	4010	3	3192	961	38
32.80	9809	3520	5	3301	893	43
37.35	9802	3134	0	3403	831	26
45.41	9915	2484	0	3473	784	21
56.65	9970	2141	0	3600	658	17

For the HD model the number of OVPs in the largest PT is very small. In particular, in the system at 56.65 GPa, the largest PT has only 17 OVPs, that is about 0.8% of all OVPs.

In summary of this section we can notice that the densification of liquid alumina was accompanied by structural change in two aspects: the proportion of basic units (AlO_4 and AlO_5) and the volume of pores and pore aggregations. The first aspect results in increasing the mean coordination number from four to six and the second one causes a decrease in diffusivity and increase in density. It is well known that diffusion in a liquid is usually performed by collective motion of all atoms and this diffusion mechanism takes place in liquid alumina. Obviously, the diffusion by the collective mechanism in the LD system was faster than the one in the HD system due to the existence of a large number of AVPs and a very large PT in the LD system. Moreover, we observed the decrease of diffusion constants with pressure in a similar way as the

volume fraction of AVPs and PT varied with pressure (see figures 8 and 11). As illustrated in figure 8 the ratio D_{Al}/D_O changed from 1.0 to 0.7. This result can be explained as follows: in the HD system most of the AVPs were eliminated, but a relatively large number of OVPs still remained in the system. Besides, the volume of the largest PT became very small, i.e. small free volume remained for collective motion of all atoms, so single-oxygen hopping (the oxygen atom can move into a neighbour OVP) became a considerable portion of diffusivity. Thereby, the oxygen diffusion constant is higher than the aluminium one. This means that the collective mechanism in the HD system also involved single-oxygen hopping.

4. Conclusions

The MD results for Al_2O_3 liquid with different densities and at 3000 K showed the structural transformation from a tetrahedral to an octahedral network. The calculation revealed that the LD system consisted mainly of AlO_4 and a small fraction of AlO_5. In contrast, in the HD system AlO_5 and AlO_6 are in a majority. The structural transformation occurred at a pressure range of 5–10 GPa, where the dynamic as well as proportion of basic units significantly changed with pressure. The diffusion mechanism also changed when liquid Al_2O_3 transformed from the LD to HD system. The Al–O–Al bond-angle distribution and fraction of different bridge-oxygen connectivities gradually changed with pressure. On the other hand, the short-range order provided by O–Al–O bond-angle and bond-length slightly changed as pressure increased from 0.14 to 56.65 GPa.

Regarding the pore and its aggregation we found that the systems with the structure of tetrahedral and octahedral networks are strongly different from each other. The LD system (tetrahedral network) has a large number of OVPs, AVPs and very large PCs (microscopic voids), and there is one PT, which includes most of the OVPs and is spread over the whole system. Meanwhile, in the HD system (octahedral network) we found only a very small number of AVPs and no microscopic void. The largest PT in the HD system involved less than 1% of the OVPs. In the region of structural transformation we observed a significant decrease in volume fraction of AVPs and the largest PT.

References

[1] Lamparter P and Kniep R 1997 *Physica* B **234–236** 405
[2] Gonzalo G 2004 *Phys. Rev.* E **69** 031201
[3] Ansell S *et al* 1997 *Phys. Rev. Lett.* **78** 464
[4] Landron C *et al* 2001 *J. Non-Cryst. Solids* **293** 453
[5] Hoang V V 2004 *Phys. Rev.* B **70** 134204
[6] Gutierrez G 2002 *Phys. Rev.* B **65** 104202
[7] Landron C *et al* 2001 *Phys. Rev. Lett.* **86** 4839
[8] Gutierrez G *et al* 2000 *Phys. Rev.* E **61** 2723
[9] Teter D M *et al* 1997 *Phys. Rev.* B **56** 5797
[10] Schweigert I V *et al* 2002 *Phys. Rev.* B **65** 235410
[11] Biswas P, Atta-Fynn R and Drabold D A 2002 *Phys. Rev.* B **69** 195207
[12] Scott Shell M, Debenedetti P G and Panagiotopoulos A Z 2002 *Phys. Rev.* E **66** 011202
[13] Lacks D J 2000 *Phys. Rev. Lett.* **84** 4629
[14] Trachenko K and Dove M T 2003 *Phys. Rev.* B **67** 064107
[15] S Han *et al* 2003 *Carbon* **41** 1049
[16] Keen D A and Dove M T 2000 *Mineral. Mag.* **64** 447
[17] Ohtaka O *et al* 2004 *Phys. Rev. Lett.* **92** 15
[18] Yasuhiro I *et al* 2004 *Phys. Rev. Lett.* **93** 015501
[19] Belonoshko A B 1998 *Phys. Chem. Mineral.* **25** 138
[20] Ahuja R, Belonoshko A B and Johansson B 1998 *Phys. Rev.* E **57** 1673

[21] Sanmigel M A *et al* 1998 *Phys. Rev.* B **58** 2369
[22] Hung P K, Nguyen P N and Belashchenko D K 1998 *Izv. Akad. Nauk SSSR Met.* **2** 118
[23] Hoang V V 2005 *Phys. Lett.* A **335** 439
[24] Hoang V V and Oh S K 2005 *J. Phys.: Condens. Matter* **17** 3025
[25] Nhan N T, Hung P K, Nghiep D M and Thang T Q 2005 Computational physics *Proc. ICCP6 and CCP2003* pp 134–8
[26] Hoang V V 2006 *Eur. Phys. J. Appl. Phys.* **33** 69–76